Enhanced gas-phase nucleation of diamond nanoparticles in a microplasma torch

Zixian Jia, Youcef Fermi, Abdoulaye Constant Siby, Ovidiu Brinza, Khaled Hassouni, Swaminathan Prasanna

Enhanced gas-phase nucleation of diamond nanoparticles in a microplasma torch

Zixian Jia[1] Youcef Fermi[2] Abdoulaye Siby[3]
Ovidiu Brinza[3] Khaled Hassouni[3]
Swaminathan Prasanna[3*]

[1] Dalian research institute of petroleum and Petrochemicals Dalian, China,
[2] Faculte des Sciences la Technologie, Universite Constantine 1, Constantine, Algeria
[3] Laboratoire des Sciences des Procédés et des Matériaux - CNRS UPR-3407 Université Paris Sorbonne Paris Nord Villetaneuse, France
[*] swaminathan.prasanna@lspm.cnrs.fr
November 15, 2022

Abstract

In this work, we present and characterize a microwave plasma microtorch that can support the formation of diamond nanoparticles (DNPs) in the gas phase when using hydrogen-methane as a precursor gas. We first showed how the non-equilibrium character of the plasma obtained in this microtorch ensures enhanced H-atom, C_2 and CH_3 production at moderate gas temperatures levels that which provides thermal stability of DNPs. The material characeterization by TEM, Raman and EELS spectra confirm the presence of substantial amount of diamond phase in the carbon dust particles collected from the plasma phase. Investigation of the effects of injected MW power on the process characteristics showed a direct correlation between enhanced C_2 production and appearance of diamond phase, which points out to the critical role of C_2 as far as gas-phase nucleation of DNPs is concerned.

Keywords: microplasma, microwave plasma, diamond nanoparticles, carbon nanostructures

1 Introduction

Nano-diamonds or Diamond nanoparticles (DNPs) are known to have outstanding properties such as superior hardness, high chemical stability and inertness to

chemical environments, high thermal conductivity, good biocompatibility and easy surface functionalization, making it suitable for a wide range of applications in the fields of medicine, tribology, catalysis, electronics and energy [26, 27, 31, 25, 8]. Further, doping the DNPs with elements such as N, Si or B in order to produce color-centers hold tremendous promise to transcend the limits of different applications in biomedical, microelectronics and quantum technologies[31, 25].

As a consequence, the synthesis of DNPs has attracted lot of attention and can be approached by several strategies such as detonation [23, 8], milling of natural or high-pressure high-temperature (HPHT) single diamond crystals, laser ablation [1], high-pressure high-temperature technique (HPHT) [30], ion irradiation of graphite [5]etc. However, major bottlenecks remain with respect to the extended adoption of DNPs as most applications demand DNPs with high quality, i.e. a low surface coverage of sp^2 hybridized carbon, and a narrow size distribution around 10 nm [31, 25]. The traditional methods of producing DNPs such as detonation [8] and milling suffer from large particle size distributions, low crystalinity and large amount of undesirable impurities [31]. Furthermore, applications based on color centers demand homogeneous distributions of dopant impurities which remains a consistent limitation of these traditional production methods [31].

In this regard, a bottom-up production strategy has been recongnized to meet the specific demands where DNPs can be nucleated from a careful selection of hydrocarbon and dopant precursors [31]. Plasma based processes can facilitate conditions supporting mild nucleation and growth of DNPs making them suitable for bottom-up strategy of producing not only pure but also doped DNPs. CVD diamond has been classically grown under microwave (MW) assisted plasmas through heterogeneous growth on a substrate that has been pre-treated or directly on single diamond crystals. These processes have been further exploited to grow micrometric sized high-quality diamond crystals with and without doping[31, 2, 6, 32]. Further investigations in the recent past have been able to demonstrate homogeneous nucleation of DNPS with a wide variety of hydrocarbon precursor gases such as methane [16], ethanol[24, 21], halogenated hydrocarbons[10, 11] etc. The carbon nanostructures produced using these gas phase nucleation processes were basically complex hybrid aggregates of graphitic carbon, amorphous carbon, and crystals of DNPs of 2-10 nm. This demonstrates that plasma process enabling homogeneous nucleation of DNPs has tremendous potential to meet the critical challenges with regard to purity, crystallinity and size distribution.

While the growth of CVD diamond films in a moderate-pressure CVD process is quite well known and understood [14], no such dedicated process and fundamental understanding of homogeneous nucleation and early growth of DNPs in plasma exists to date. As a matter of fact, while CH_3 and H-atom have been recognized as key species in the growth of CVD diamond [14, 20], there is no such agreement in the litterature on the key species that induce early nucleation of nanodiamond in the gas phase or on solid substrates [14]. Early studies on nanocrystalline diamond (NCD) deposition mentionned the key-role that may

be played by C_2 as a driver for the nucleation of nanocristalline sp^3 domain [17] . On the same line, Dolmatov et al. [8] speculate that C_2 may be the key primary radical responsible for the nucleation and growth of DNPs by detonation process. According to these authors, the highly reactive C_2 radicals react with themselves to form cyclo-hexane which subsquently undergo further molecular growth involving methyl radical and H-atom, just like in the case of classical CVD diamond, to form sp^3 carbon diamondoid structures. In summary, these investigations show that the production of diamond nanoparticles in the gas phase requires a nucleation step that is likely driven by C_2 along with early growth step that requires CH_3 radical and H-atom. Besides, the production of DNPs in the plasma phase requires local plasma characterisrtics that meet the stability conditions for DNPs once nucleated. In particular, the gas temperature should be moderate, typically below 2000k, in order to avoid graphitization[7].

It appears therefore that the production of diamond nanoparticles in the plasma phase requires plasma conditions that enhance C_2, CH_3 and H-atom production while keeping moderate gas temperature. Such conditions can be hardly met in classical diamond plasma CVD systems that were specifically designed to achieve large CH_3/H densities with a little attention to C_2 production and where the gas temperature level is generally not optimal as far as DNPs stability is concerned. This point partly motivates our objective to develop a novel plasma process that is suitable for gas phase production of DNPs. Our strategy is to use the peculiarity of microplasmas that provide very high electron density thus enhancing the electron driven production of a variaty of H-C radicals and H-atom under fairly moderate gas temperatures. More specifically, we report the preliminary results on the synthesis of DNPs in a MW assisted microplasma torch using a gas mixture of hydrogen and methane. We will first present the MW-plasma device developed in this work and its characterization in terms of gas temperature, electron and H-atom densities. Then, in the second part of the paper, we will discuss the characteristics of the carbanaceous materials synthesized in the torch and discussing its characteristics which clearly shows the gas phase nucleation of diamond nanoparticles. We will eventually end up the paper by discussing the obsreved correlations between the plasma and material characteristics

2 MW plasma torch characterization

The 2.45 GHz MW plasma microtorch (Figure 1) was developed in-house and is based on coaxial transmission line resonator (CLTR) coupling techniques[4]. The length of the coaxial resonator is approximately equal to $3\lambda/4$ which facilitates the electromagnetic resonance at one end of the torch. Further, a small gap distance of 250 μm at the end of the torch, between the central brass rod and the annular grounded head, coupled with effect of resonance ensures a strong electromagnetic field that sustains the plasma. The as created plasma volume is very small ($O(mm^{-3})$ resulting in MW power densities as high as 5×10^9 W/m^{-3}, which is three orders of magnitude greater than in a conventional

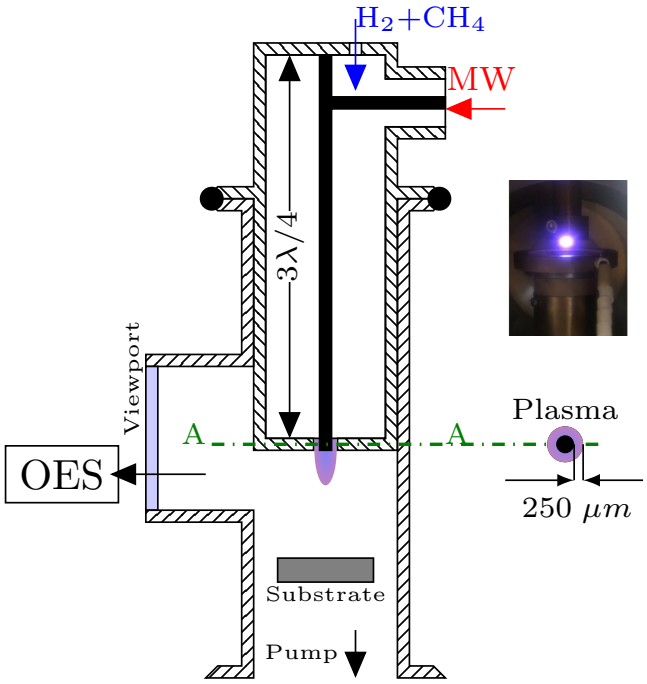

Figure 1: MPCVD reactor and OES set up

CVD reactor used for diamond growth[29]. This provides a distinct advantage for producing highly non-equilibrium discharges with high electron densities and moderate gas temperatures which can realize a wide range of reactive environments with charged species, radicals and photons over dimensions limited to few millimetres. The present torch can be operated with different gas mixtures such as argon, hydrogen, methane, acetylene and ethanol, and over a wide range of pressure conditions (10 mbar – 1 atm). Nevertheless, in this paper we will restrict our discussion to a precursor gas mixture composition of H_2 (96%) and methane (4%) and an operating pressure of 100 mbar where substantial amount of diamond nanoparticles were produced.

The local plasma conditions such as rotational temperature, electron and H-atom density, were characterized using optical emission spectrocopy (OES) with the help of spectrometers having 1 m (THR1000) and 2m (SOPRA) focal lengths. The latter spectrometer was used only for electron density measurements where highly resolved line profile monitoring is required. The gas temperature, which may be inferred from the rotational temperature, and the electron density and temperature are the main driver of the gas phase chemistry. In our experiments, the Q-branch of H_2 Fulcher-α band was used to estimate the H_2 rotational temperatures from the slope of the Boltzmann plot corresponding to the selected rotational lines Q1, Q2, Q3 and Q6 (Fig. S1). It is expected

that for the moderate pressure conditions used in our experiments, the upper excited states $d^3\prod_u$ of Fulcher band would undergo collisions before raditative de-excitation. Therefore, the use of the lower state rotational constant for determining the rotational temperature as commonly used for very low pressure plasma is questionable. On the otherhand the use of the upper state rotational constant to determine the temperature requires full equilibriation of the rotational mode of the excited levels which is not guaranted in our conditions. Also, other spectroscopic bands such as the R branch of the transition $G^1\sum_g$, $\nu' = 0 \rightarrow B^1\sum_u^+$ of H_2 or Swann band of C_2 which can also give information on the gas temperature, were unfortunately not accessible for the discharge conditions of interest. We therefore estimated upper- and lower-limit values of the rotational temperature corresponding to two asymptotic situations : negligible collision effect and full rotational equilibration of the excited states, respectively. The actual gas temperature is expected between these two limits.

In fact, taking into account the collisional cross-section of $d^3\prod_u$ $2\times10^{-15}cm^{-2}$ [12], the collisional and radiative lifetimes are comparable i.e. 50 ns and 60 ns respectively . This means that the excited states are likely to undergo few collisions before radiative deexcitation. Consequently, the gas temperature is likely to be much closer to the upper limit. As shown in Fig. 2, the lower and upper limits fo the rotational temperature increase from 525 to 760 K and from 1000 to 1500 K respectively, when the injected power increases from 30 to 90 W. Most importantly, the gas temperature remains below 1500 K which avoids graphitization of nanodiamond in the plasma phase. The limited gas heating that characterize our system is due to the large surface to volume ratio and the effective cooling of the torch.

Electron density were estimated from the stark broadening of the H_β line [15] that was captured using the 2m focal length spectrometer SOPRA (c.f. Figure S2). For our plasma conditions, the broadening of H_β line is well represented by a voigt profile where the Gaussian component comprises of the instrumental and Doppler broadening while the Lorentzian component includes Van der Waals and, more importantly, Stark broadenings. The Doppler and Van der Waals line-widths were estimated using the H_2 rotational temperature. Typical values for these were 9 and 5 pm respectively. Using the mercury line at 576 nm, the instrumental broadening was estimated as 7.66 pm. The Stark linewidth of H_β line obtained by eliminating the instrument, Doppler and Van der Waals line-widths is about 10 pm. It is clear that the broadening is dominated by Stark effect and therefore the uncertainty in the gas temperature does not affect the electron density substantially. The electron densities remained constant with injected MW power with typical values of 2×10^{13} cm^{-3} (c.f. Figure S3). This is two orders of magnitude greater than the values measured in a conventional resonating MW reactor used for CVD growth of diamond[19]. The direct consequence of such high electron densities is enhancement of electron impact processes.

H-atom density was determined by performing H-atom actinometry [13] where trace amounts of Ar (1%) are added without altering the plasma char-

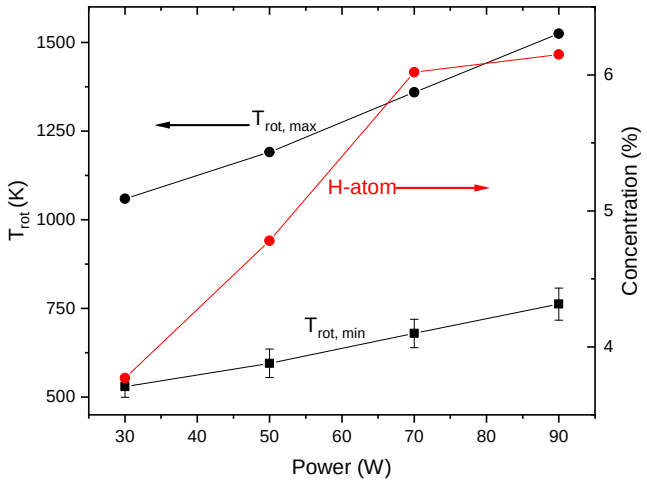

Figure 2: Lower and upper limits of H_2 rotational temperature measured from the OES spectra of Q-branch of H_2 Fulcher-α band and concentration of H-atoms measured by actinometry [13] as a function of input microwave power.

acterisitics. The H-atom densities are inferred directly from the ratio of line intesities of H_α to Ar line at 750 nm using the calibration method thoroughly described in [13]. Large concentrations of H-atom of about 6% (c.f. Fig. 2) was found in our conditions which are of the same order of magnitude to that obtained in the resonant MW cavity used for diamond CVD. However, unlike in the case of resonant cavity MW reactor where the thermal processes are responsible for the dissociation of hydrogen , the gas temperature in our conditions is not high enough to induce thermally driven dissociation, and the H-atom production is mainly ensured by the electron impact processes.

As for hydrocarbon molecules, we could detect strong emission from the Swann molecular band of C_2, the intensity of which increased with the input MW power. Unfortunately, we could not detect the emission lines from CH molecules that could be used as an indicator for the concentration of CH_3 in our conditions. Therefore, we adapted the 0D model described in [18] to our conditions in order to estimate the densities of key hydrocarbon species, especially C_2 and CH_3. The results from the simulations indicate a substantial increase in the concentrations of CH_3 and C_2 with MW power as seen in Figure 3(b). H-atom and electron rich conditions are responsible for the formation of CH_3 radical through both the H-shifting and electron impact reactions of CH_4 that produces CH_3 radical. The production of C_2 through thermal processes is very unlikely for the gas temperature values that characterize our plasmas. However, the very high electron densities in our conditions strongly enhance the formation of this radical through electron impact on intermediate hydrocarbon species such as C_2H_2 and C_2H_4 that are effectively produced thermally in the gas temperature range that characterizes our plasma [19]. As a result, the concentration of C_2

is comparable with that of CH_3 at 90 W which shows that these species can indeed play a key-role in hydrocarbon molecular growth and subsequent carbon nanoparticle nucleation as suggested by several studies and discussed in the next section for our discharge conditions.

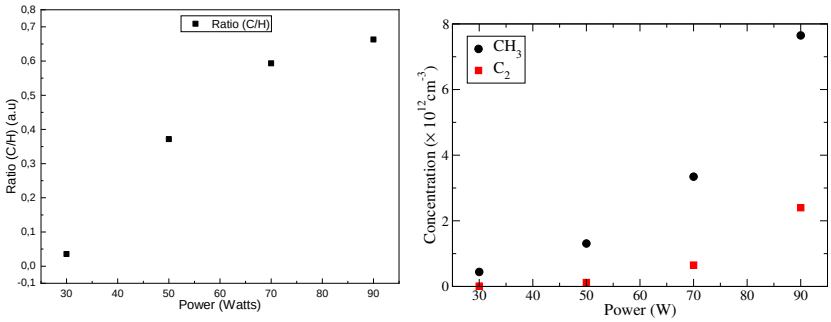

Figure 3: (a) The relative abundance of C_2 radical to H-atom concentration evaluated from the ratio of intensities of I(C_2 Swann) and H-alpha and (b) Concentrations of C_2 and CH_3 from 0D-global model as a function of input power

3 Carbon nanostructure characterization

The carbon nanostructures produced in our discharge were collected on a substrate placed down stream the reactor. A variety of carbon nanostructures have been collected for different precursor feed gas compositions (Argon + Hydrogen and methane), working pressure and injected MW power.

Scanning electron microscopy (SEM) (Zeiss Supra 40 VP SEM-FEG) was used to characterize the morphology of carbon nanoparticles while TEM observation was performed in a JEOL 200 kV microscope with the carbon nanoparticles suspension drop-casted onto a carbon TEM grid. The Raman spectra of the samples at room temperature were measured in the backscattering configuration using a HR800 spectrometer equipped with a Peltier-cooled CCD detector (Horiba Jobin Yvon) with spectral and spatial resolutions of 0.25 cm^{-1} and 5 μm, respectively. Raman measurements were carried out by focusing the probe beam at 473 nm with a 50x objective on the carbon particles.

Material characterization using SEM (Figure S4) and TEM indicated an agglomerated nanostructures deposit with particle size around 10 nm. EDX shows that the nanostructures contain predominantly C with traces of O and Si due to pollution from the substrate during the characterization(c.f. Fig S4). Figure 4 shows the TEM images and their corresponding electron diffraction pattern for the carbon nanostructures collected at power of 90 W. Under these conditions, hybrid nanostructures containing both graphitic carbon and diamond were observed as seen in Fig 4a. The d-spacings of 0.21 nm and 0.35 nm are consistent

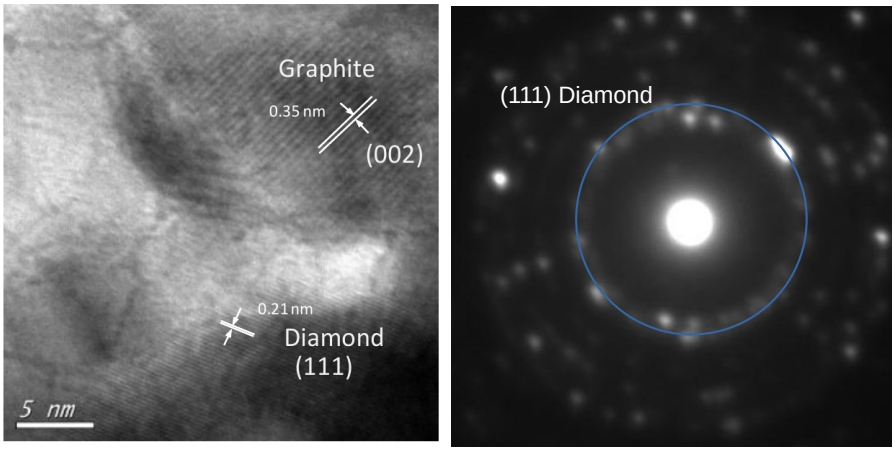

Figure 4: TEM image of carbon nanoparticles at resolution of 1.8 A and its corresponding (b) selected area electron diffraction with blue circle refers to the (111) plane of diamond phase. (Experimental conditions: CH4 = 4 sccm, H2 = 96 sccm, Pressure of reactor = 100 mbar, Injected power = 90 W)

with diamond (111) planes and graphite (002) planes, respectively. The crystaline nature of the collected carbon nanostructres is further confirmed by the observation of concentric rings in the electron diffraction patterns with strong indication of diamond phase as seen in Fig 4b. EELS spectra in Fig. 5 show the 1s $\sigma*$ bond which correspond to sp^3-hybridised carbon. The presence of some amounts of sp^2 carbons is also indicated by 1s $\pi*$ feature. This establishes that the diamond nanoparticles along with impurities of sp^2 hybridized and other amorphous carbon are formed in these conditions.

Figure 6 shows the evolution of the raw and fitted Raman spectra (obtained with a laser excitation at 473 nm) of the carbon nanostructures collected on a silicon substrate placed at a distance of 1 cm from the plasma for different absorbed MW power. The quantity of collected carbon nanostructures increases with the MW power. Prominent peaks of sp^2 carbon i.e. D peaks at 1280 and 1385 cm^{-1} and G peak at 1598 cm^{-1} are present for all the conditions [9]. The diamond peak located around 1332 cm^{-1} appeared in the Raman spectra of the carbon nanostructures only for MW powers above 70 W. For bulk diamond with high crystalline quality, this peak is usually sharp. The diamond nanoparticles obtained in our conditions are however of nm-sized grains. As a consequence, due to phonon confinement, an asymmetrical broadening was observed on this diamond peak which was blue shifted to 1329 cm^{-1}[22]. In addition to this, the Raman spectra shows a peak around 1129 cm^{-1} which is associated with the μ_1 mode of transpolyacetylene [9] and the ratio of this peak to the G-peak increased with MW power.

From the Raman spectra, the ratio of Diamond peak at 1332 cm^{-1} and sp^2 carbon G-band is used to access the trends of sp^3/sp^2 ratio. Figure 7 shows the

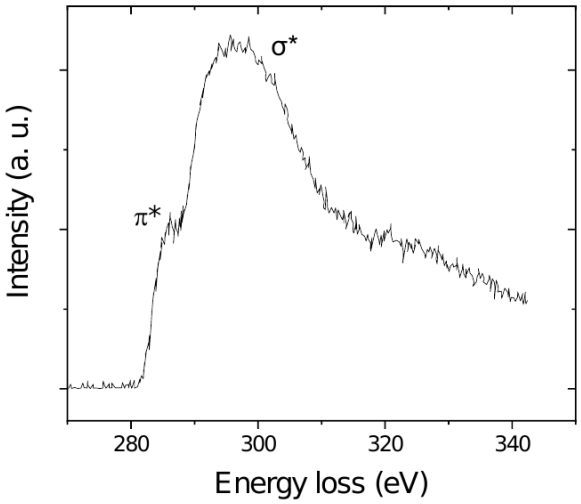

Figure 5: EEEL spectra of carbon nanoparticles (Experimental conditions: CH4 = 4 sccm, H2 = 96 sccm, Pressure of reactor = 100 mbar, Injected power = 90 W)

variation of ratios of sp^3/sp^2 content and I_D/I_G with the absorbed MW power. The power has a positive effect on sp^3 carbon formation. In addition, the I_D/I_G ratio decreases from 0.53 to 0.33 with increasing power. Similar results reported in the literature also show that I_D/I_G ratio decreases with increasing sp^3 fraction in the amorphous carbon films [28][3].

Growth of carbon nanostructures can follow two different pathways (i) homogeneous nucleation in the gas phase or (ii) heterogeneous growth at the surface of the substrate. While homogeneous nucleation is driven by gas phase molecular growth and nucleation, the heteregeneous growth is driven by surface stabilization offered by the substrate as observed during the CVD growth of diamond. The signature of carbon nanostructures produced in our experiments was insensitive to the nature of the different substrates used such as silicon and fibre glass. Moreover, there was no pre-treatment of the substrate whose temperature was almost constant (340 K) in all the experiments. The signature of the Raman spectra of the carbon nanostructures collected were very similar when the distance between the substrate and the plasma was varied in the range 2.5 mm and 2 cm. Similarly, this was true with respect to the carbon nanostructures collected over a wide range of deposition duration, i.e., 5 to 60 minutes. All these experimental facts clearly show that the the nucleation of DNPs in our discharge occurs in gas phase. However, we cannot rule out the possibility of subsequent evolution of homogeneously nucleated DNPs containing nanostructures, once deposited on the susbtrate.

When correlating the results of plasma and material characterization, one can clearly see that the production of DNPs in the gas phase takes place when

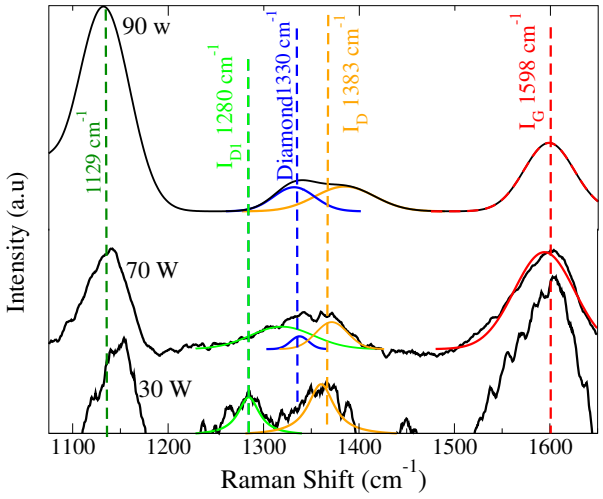

Figure 6: The Raman spectra of the samples obtained with different powers: 30W, 70W and 90W Also shown are the different components of the spectra: Diamond peak at 1330 cm^{-1} (blue line), D-peak at 1280 (Green line) and 1385 cm^{-1} (Orange line), G peak at 1598 cm^{-1} (red line) and peak at 1129 cm^{-1} corresponding to transpolyacetylene.

C_2 and CH_3 densities are strongly enhanced, i.e. basically for a power value above 70 W. In particular, no DNPs were observed despite the existence of significant amount of H-atom and substantial amount of CH_3 at low MW injected power. Therefore, our results tend to confirm that the existence of a substantial amount C_2 is required to nucleate DNPs in gas phase. Most probably, C_2 radical is responsible for the formation of small hydrocarbon structures which act as seeds that further grow through the classical mechanism involving CH_3 and H. Examples of such structures and their formation mechanism from C_2 have been suggested in [8]. Unfortunately, the increase in C_2 is accompanied by the enhancement of transpolyacetylene which is initiated by C_2 radical through polymerization that results in unsaturated carbon chains such as (-C*=C*-). Moreover, the H-atom rich conditions further stabilize these large transpolyacetylene structures. This shows that optimal conditions of DNPs gas phase production requires finding the discharge conditions that inhibits the formation of polyacetylene structures while still ensuring large enough C_2 density to produce molecular structures that lead to nucleation of DNPs.

4 Conclusion

We have constructed a MW microplama source which can produce conditions that favour the homogeneous nucleation of DNPs. Specifically, the high-electron densities that characterize our microplasma provided H-atom, C_2 and CH_3 rich

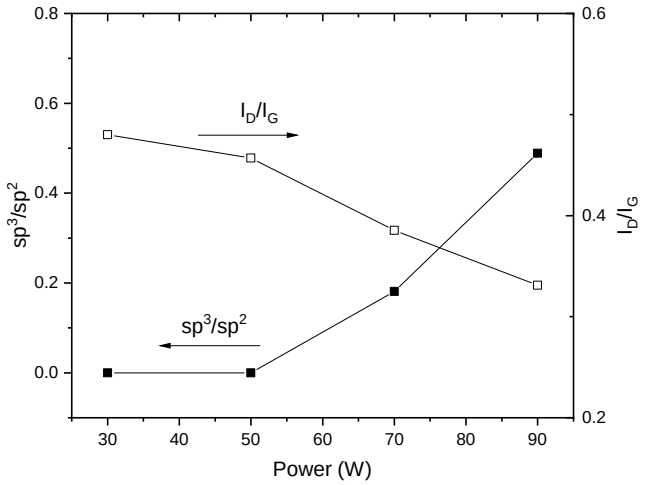

Figure 7: the sp^3/sp^2 (left) and I_D/I_G (right)ratio as a function of input power (sp^3/sp^2 bonds ratio is calculated from the intensity of the diamond peak at 1328 cm^{-1}, the intensity of the G band about 1583 cm^{-1})

conditions with moderate gas temperatures that can support molecular growth pathways which end up with nucleation of DNPs. The correlation between the results of plasma diagnostics and material characterization clearly indicates the importance of carbon radicals C_2 and CH_3. Particularly, the direct correlation between the appearance of diamond phase and enhanced concentrations of C_2 at high MW power points to the critical role played by C_2 during the early molecular growth that leads to DNPs nucleation.

Further research is needed to identify the intermediate HC species that are involved in the molecular growth mechanism leading to DNPs. This may be achieved using molecular beam mass spectrometry. Also, substantial improvement of the plasma phase DNP production proces is possible by limiting the competetive formation of transpolyacetylene under C_2 rich conditions that are also required for DNPs nucleation.

References

[1] David Amans, Anne-Claire Chenus, Gilles Ledoux, Christophe Dujardin, Cecile Reynaud, Olivier Sublemontier, Karine Masenelli-Varlot, and Olivier Guillois. Nanodiamond synthesis by pulsed laser ablation in liquids. *Diamond and Related Materials*, 18(2-3):177–180.

[2] Michael NR Ashfold, Jonathan P Goss, Ben L Green, Paul W May, Mark E Newton, and Chloe V Peaker. Nitrogen in diamond. *Chemical reviews*, 120(12):5745–5794.

[3] Y Cai, RY Wang, HD Liu, C Luo, Q Wan, Y Liu, H Chen, YM Chen, QS Mei, and B Yang. Investigation of (ti: N)-dlc coatings prepared by ion source assisted cathodic arc ion-plating with varying ti target currents. *Diamond and Related Materials*, 69:183–190.

[4] J Choi, F Iza, HJ Do, JK Lee, and MH Cho. Microwave-excited atmospheric-pressure microplasmas based on a coaxial transmission line resonator. *Plasma Sources Sci. Technol.*, 18(2):025029.

[5] TL Daulton, MA Kirk, RS Lewis, and LE Rehn. Production of nanodiamonds by high-energy ion irradiation of graphite at room temperature. *Nuclear Instruments and Methods in Physics Research Section B: Beam Interactions with Materials and Atoms*, 175:12–20.

[6] Mary De Feudis, Alexandre Tallaire, Louis Nicolas, Ovidiu Brinza, Philippe Goldner, Gabriel Hétet, Fabien Bénédic, and Jocelyn Achard. Large-scale fabrication of highly emissive nanodiamonds by chemical vapor deposition with controlled doping by siv and gev centers from a solid source. *Advanced Materials Interfaces*, 7(2):1901408.

[7] Alessandro De Vita, Giulia Galli, Andrew Canning, and Roberto Car. Graphitization of diamond (111) studied by first principles molecular dynamics. *Applied surface science*, 104:297–303.

[8] V Yu Dolmatov, Aleksandr Nikiforovich Ozerin, Inna Ivanovna Kulakova, Olexandr Olexandrovich Bochechka, Natalia Mikhailovna Lapchuk, Vesa Myllymäki, and Asko Vehanen. Detonation nanodiamonds: new aspects in the theory and practice of synthesis, properties and applications. *Russ. Chem. Rev.*, 89(12):1428.

[9] Andrea C Ferrari and John Robertson. Resonant raman spectroscopy of disordered, amorphous, and diamondlike carbon. *Physical review B*, 64(7):075414.

[10] MRDWKE Frenklach, R Kematick, Do Huang, Wo Howard, KE Spear, Ao W Phelps, and R Koba. Homogeneous nucleation of diamond powder in the gas phase. *J. Appl. Phys.*, 66(1):395–399.

[11] MWDJKER Frenklach, W Howard, D Huang, J Yuan, KE Spear, and R Koba. Induced nucleation of diamond powder. *Applied physics letters*, 59(5):546–548.

[12] RK Garg, TN Anderson, RP Lucht, TS Fisher, and JP Gore. Gas temperature measurements in a microwave plasma by optical emission spectroscopy under single-wall carbon nanotube growth conditions. *J. Phys. D: Appl. Phys.*, 41(9):095206.

[13] a. Gicquel, M. Chenevier, Kh. Hassouni, a. Tserepi, and M. Dubus. Validation of actinometry for estimating relative hydrogen atom densities and

electron energy evolution in plasma assisted diamond deposition reactors. *J. Appl. Phys.*, 83(1998):7504.

[14] Alix Gicquel, Khaled Hassouni, François Silva, and Jocelyn Achard. Cvd diamond films: From growth to applications. *Curr. Appl Phys.*, 1(6):479–496.

[15] Marco A. Gigosos, Manuel Ã. GonzÃ¡lez, and ValentÄ±Ìn CardeÃ±oso. Computer simulated balmer-alpha, -beta and -gamma stark line profiles for non-equilibrium plasmas diagnostics. *Spectrochimica Acta Part B: Atomic Spectroscopy*, 58(8):1489–1504. 5th European Furnace Symposium and 10th International Solid Sampling Colloquium with Atomic Spectroscopy.

[16] T Gries, L Vandenbulcke, JN Rouzaud, and S De Persis. Diagnostics in dusty c–h–o plasmas with diamond and graphitic nanoparticle generation. *Plasma Sources Sci. Technol.*, 19(2):025015.

[17] Dieter M Gruen, Chris D Zuiker, Alan R Krauss, and Xianzheng Pan. Carbon dimer, c2, as a growth species for diamond films from methane/hydrogen/argon microwave plasmas. *Journal of Vacuum Science & Technology A: Vacuum, Surfaces, and Films*, 13(3):1628–1632.

[18] K Hassouni, X Duten, A Rousseau, and A Gicquel. Investigation of chemical kinetics and energy transfer in a pulsed microwave h2/ch4 plasma. *Plasma Sources Sci. Technol*, 10:61–75.

[19] K. Hassouni, F. Silva, and A. Gicquel. Modelling of diamond deposition microwave cavity generated plasmas. *J. Phys. D: Applied Physics*, 43:153001.

[20] M Heintze, M Magureanu, and M Kettlitz. Mechanism of c 2 hydrocarbon formation from methane in a pulsed microwave plasma. *Journal of applied physics*, 92(12):7022–7031.

[21] Saman Iqbal, Muhammad Shahid Rafique, Muhammad Zahid, Shazia Bashir, Muhammad Ashfaq Ahmad, and Rabia Ahmad. Impact of carrier gas flow rate on the synthesis of nanodiamonds via microplasma technique. *Mater. Sci. Semicond. Process.*, 74:31–41.

[22] Vitaly I Korepanov, Hiro-o Hamaguchi, Eiji Osawa, Vladimir Ermolenkov, Igor K Lednev, Bastian JM Etzold, Olga Levinson, Boris Zousman, Chandra Prakash Epperla, and Huan-Cheng Chang. Carbon structure in nanodiamonds elucidated from raman spectroscopy. *Carbon*, 121:322–329.

[23] Anke Krüger, Fumiaki Kataoka, MAA Ozawa, T Fujino, Y Suzuki, Aleksandr E Aleksenskii, A Ya Vul, and Eiji Ōsawa. Unusually tight aggregation in detonation nanodiamond: identification and disintegration. *Carbon*, 43(8):1722–1730.

[24] Ajay Kumar, Pin Ann Lin, Albert Xue, Boyi Hao, Yoke Khin Yap, and R Mohan Sankaran. Formation of nanodiamonds at near-ambient conditions via microplasma dissociation of ethanol vapour. *Nature communications*, 4:2618.

[25] Sandeep Kumar, Monika Nehra, Deepak Kedia, Neeraj Dilbaghi, K Tankeshwar, and Ki-Hyun Kim. Nanodiamonds: Emerging face of future nanotechnology. *Carbon*, 143:678–699.

[26] Vadym N Mochalin, Olga Shenderova, Dean Ho, and Yury Gogotsi. The properties and applications of nanodiamonds. *Nature nanotechnology*, 7(1):11.

[27] Nicholas Nunn, Marco Torelli, Gary McGuire, and Olga Shenderova. Nanodiamond: a high impact nanomaterial. *Curr. Opin. Solid State Mater. Sci.*, 21(1):1–9.

[28] Namwoong Paik. Raman and xps studies of dlc films prepared by a magnetron sputter-type negative ion source. *Surface and Coatings Technology*, 200(7):2170–2174.

[29] Swaminathan Prasanna, Armelle Michau, Cathy Rond, Khaled Hassouni, and Alix Gicquel. Self-consistent simulation studies on effect of methane concentration on microwave assisted h2-ch4 plasma at low pressure. *Plasma Sources Sci. Technol.*, 26(9):097001.

[30] J Qian, C Pantea, J Huang, TW Zerda, and Y Zhao. Graphitization of diamond powders of different sizes at high pressure–high temperature. *Carbon*, 42(12-13):2691–2697.

[31] Olga A Shenderova, Alexander I Shames, Nicholas A Nunn, Marco D Torelli, Igor Vlasov, and Alexander Zaitsev. Synthesis, properties, and applications of fluorescent diamond particles. *Journal of Vacuum Science & Technology B*, 37(3):030802.

[32] Alexandre Tallaire, Ovidiu Brinza, Paul Huillery, Tom Delord, Clément Pellet-Mary, Robert Staacke, Bernd Abel, Sébastien Pezzagna, Jan Meijer, Nadia Touati, Laurent Binet, Alban Ferrier, Philippe Goldner, Gabriel Hetet, and Jocelyn Achard. High nv density in a pink cvd diamond grown with n2o addition. *Carbon*, 170:421–429.

Acknowledgements

“ANR (Agence Nationale de la Recherche) and CGI (Commissariat à l’Investissement d’Avenir) are gratefully acknowledged for their financial support of this work through Labex SEAM (Science and Engineering for Advanced Materials and devices), ANR-10-LABX-0096 and ANR-18-IDEX-0001”. One of the author (Khaled Hassouni) acknowledge the support of the Institut Universitaire de France.

5 Supplementary Material

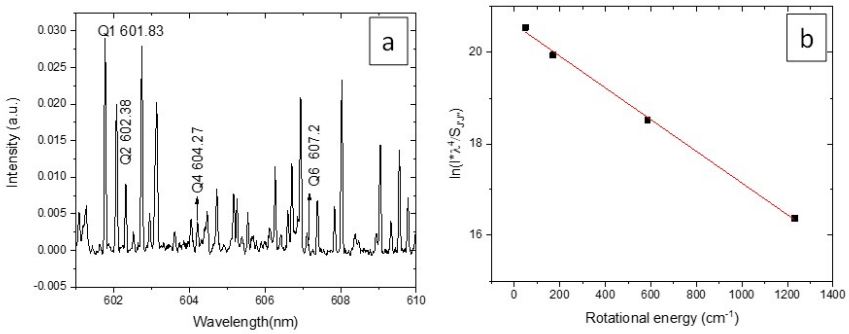

Figure S1: (a) Example of measured H_2 Fulcher-α Q-branch spectrum with indication to the selected rotational lines and (b) the corresponding Boltzmann plot, at microwave power of 70 W and pressure of 100 mbar.

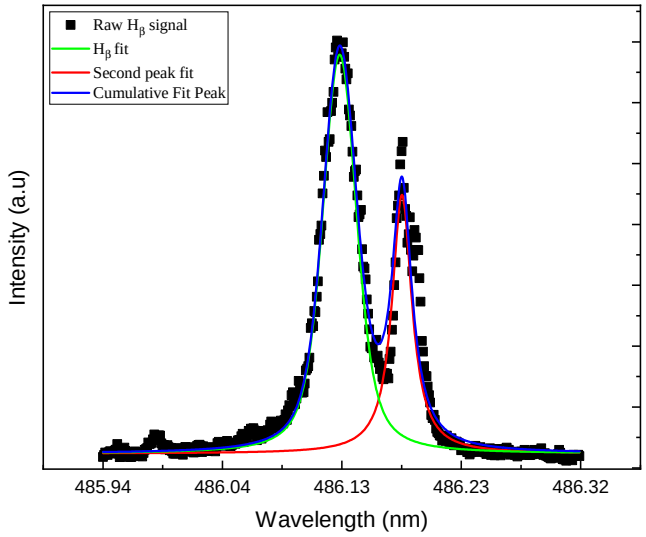

Figure S2: Example of raw H_β spectrum and its corresponding fits obtained at 90 W and pressure of 100 mbar. Also seen is a parasitic line caused by Cu^{2+} which must be present in the gas phase due to etching of the brass pin by hydrogen.

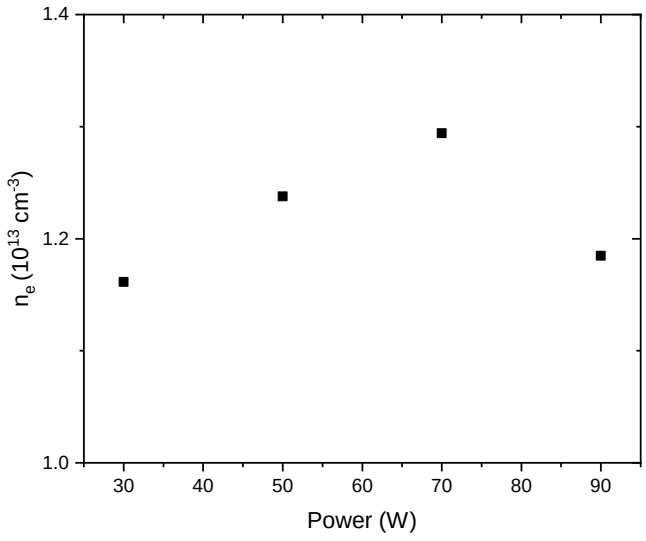

Figure S3: Electron densities measured from Stark broadening of H_β as a function of input MW power.

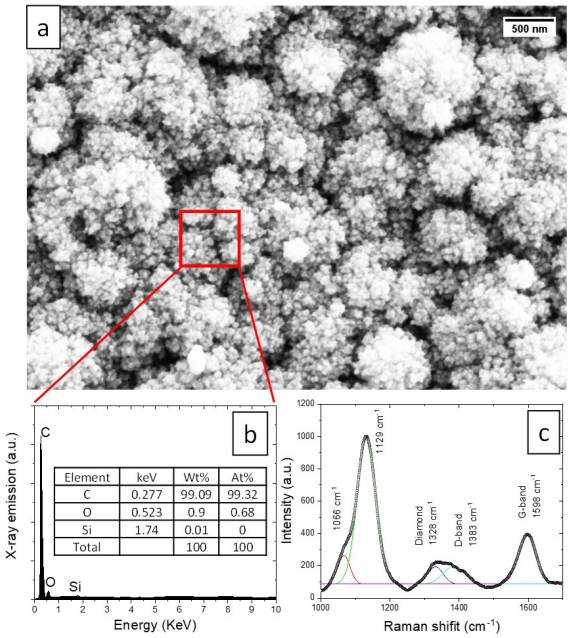

Figure S4: Material characterization of carbon nanoparticles deposited on Si substrate. a) SEM image carbon nanoparticles, b) its corresponding EDX spectra, and c)Micro Raman spectra. (Experimental conditions: CH4 = 4 sccm, H2 = 96 sccm, Distance between plasma torch and substrate = 5mm, Frequency of microwave =2480 Hz, Pressure of reactor = 100 mbar, Injected power = 90 W, Deposition time = 60 min)